CAAP Quarterly Report

Date of Report: July 10, 2016

Contract Number: DTPH5615HCAP03

Prepared for: James Prothro, PHMSA-DOT

Project Title: Bayesian Network Inference and Information Fusion for Accurate Pipe Strength and Toughness Estimation

Prepared by: Arizona State University, University of Colorado-Denver

Contact Information: Dr. Yongming Liu and Dr. Yiming Deng

For quarterly period ending: April 10, 2016

Business and Activity Section:

ASU Student training activities

- Sonam Dahire works on the material specimen preparation, testing, and data analysis;
- Sonam Dahire and Tishun Peng work on the Bayesian inference with experimental measurements;
- Ankita Kardile works on the numerical and experimental testing for the ABI testing for strength estimation;
- Sonam Dahire and Ankita Kardile write the report.

CU Denver student training activities

- Xiaodong Shi works on multi-physics modeling, numerical algorithms development and analysis, as well as fast continuous imaging protocol design and implementation
- Salem Egdaire works on NMMI amplitude and phase imaging development Xiaodong Shi and Deepak Kumar works on the experimental testing for data fusion and correlations between electromagnetic measurements and mechanical measurements
- Deepak Kumar works on the compressed sensing assisted fast imaging development
- Xiaodong Shi and Deepak Kumar write the report

(a)Generated Commitments

The system for natural gas pipelines in the United States consists of a network to gather, transport and distribute the product, which consists of 210 systems overall running through the different states. Pipeline infrastructure forms a vital aspect in improving the U.S. economy and standard of living A major portion of the current operational pipelines have been installed in the early 1900's, and therefore lack reliable information on the integrity of the aging pipeline systems which is a critical safety concern. The conventional methods of inspection such as pipeline inspection gauge (PIG) cannot be used to inspect about three-fourth of the present pipeline systems, due to the pipes being too old/ twists/turns etc. which does not allow PIGs to operate in them. In order to maintain the safety and economy standards, accurate estimation of pipe strength and toughness without interrupting the transmission and operations of the pipelines is crucial. Many of the existing techniques focus on single modality measurement for the narrow surface layer measurements and cannot capture decarburization and manufacturing process-induced material inhomogeneity. Also, uncertainties exist in terms of material properties, pipe geometries, manufacturing process, operational conditions, etc., leading to gaps in the accurate strength and toughness determination. Therefore, a novel approach using multimodality diagnosis and information fusion framework has been proposed for probabilistic pipe strength and toughness estimation, which is the objective of the present work. The first part of the project will consist of estimating the basic material properties; microstructure, composition etc. as well as various surface mechanical properties and studying their variation with thickness of the pipeline samples. The second part compromises of advanced testing methods for property estimation with the use of acoustic and electromagnetic sensors. And finally, the information obtained from the two parts would be integrated with the statistical correlations into a multimodal system to obtain a probabilistic strength and toughness with a high degree of accuracy. The typical pipeline grades include A, B, X42, and X46 as distribution pipelines, and X52, X56, X60, X65, X70, X80 etc. for transmission. The latter grades such as X65-X120 have been manufactured through advanced processing methods which imparts a better control on the mechanical properties. However, due to the conventional processing methods for the earlier grades, a large variation in the properties has been observed. These earlier grades still form a vital part of the current service pipelines, hence, a reliable source of information of the aging systems is essential, and therefore form the focus of our study.

Several major tasks are proposed to address the above-mentioned project objectives/goals. Experimental testing, advanced data analysis, numerical simulation, and probabilistic methods are integrated in the proposed tasks. A summary is listed below and detailed work plan will be discussed in the following sections.

Task 1. Experimental testing and data analysis of chemical, metallurgical, and mechanical properties of pipe steel (Arizona State University)

This task focuses on the information obtaining and analysis about the basic pipe steel properties. Both in-house experimental testing and literature data will be used for this task. First, in situ and ex situ chemical composition analysis will be performed for several representative pipe steel specimens (from online vendors and our industry collaborators). Optical emission spectrography (OES) and energy dispersive spectroscopy (EDS) will be used for in situ and ex situ measurements of chemical composition, respectively. Following this, in situ and ex situ pipe steel microstructure analysis will be performed to obtain the grain structure images using etchingbased optical microscopy and electron back scattered diffraction (EBSD) images, respectively. Imaging analysis will be performed to obtain the statistical information and metrics about the pipe steel microstructure, such as grain size distribution. Next, surface hardness measurements will be performed using portable ultrasound hardness testers and the results will be correlated with pipe strength and toughness. Advanced data analysis using Gaussian Process modeling will be used for surrogate modeling and to quantify the uncertainties for future Bayesian network inference.

Task 2. Experimental testing, data analysis and prototyping for acoustic and microelectromagnetic electromagnetic properties of pipe steel (University of Colorado-Denver)

This task focuses on the information obtaining and analysis about the pipe steel acoustic and microelectromagnetic properties. First, ex situ low-frequency near-field microwave microscopy analysis will be performed for several representative pipe steel specimens. Obstacles for dislocation movement, such as grain boundaries and void inclusions, will be revealed in terms of measurable electromagnetic properties. Following that, surface and subsurface microstructural image analysis assisted by Multiphysics modeling will be carried out to understand the correlations between steel strength and different possible mechanisms which impede the dislocation movement under load in the micro electromagnetic spectrum. Next, a prototype of integrating magnetostriction and pulsed eddy current-based Barkhausen noise imaging system will be developed to characterize the pipe steel's Bloch wall jumps and the results will be correlated with pipe strength and toughness experimentally with advanced data analysis.

Task 3. Bayesian network for information fusion and probabilistic pipe strength estimation (Arizona State University and University of Colorado-Denver)

This task will focus on the development of a novel Bayesian network for the inference of pipe strength and toughness. First, the network structure and conditional probability estimation will be performed using the multi-modality diagnosis data obtained in Tasks 1&2. Following this, parametric studies with synthetic data using the developed Bayesian network will be performed to investigate the behavior and performance of the information fusion framework. Sensitivity analysis will be performed to identify the important factors in the proposed Bayesian network. Finally, model verification and

validation with realistic field/laboratory measurements will be demonstrated. Probabilistic pipe strength estimation and associated risk-based confidence determination will be quantified.

A schematic illustration of the proposed components and their integration is shown in Fig.1. The philosophy behind the proposed methodology is that each modality diagnosis will contain part of the information about the pipe steel strength and a fusion process will, in principle, provide more accurate estimation of the current state of the aging pipes. This schematic illustration also indicates the multidisciplinary collaborative work of the proposed study. Mechanical and material research (ASU), electromagnetic and acoustic study (CU-Denver), and industrial experiences (GTI) are integrated together for the probabilistic pipe strength estimation and future decision making for risk mitigation.

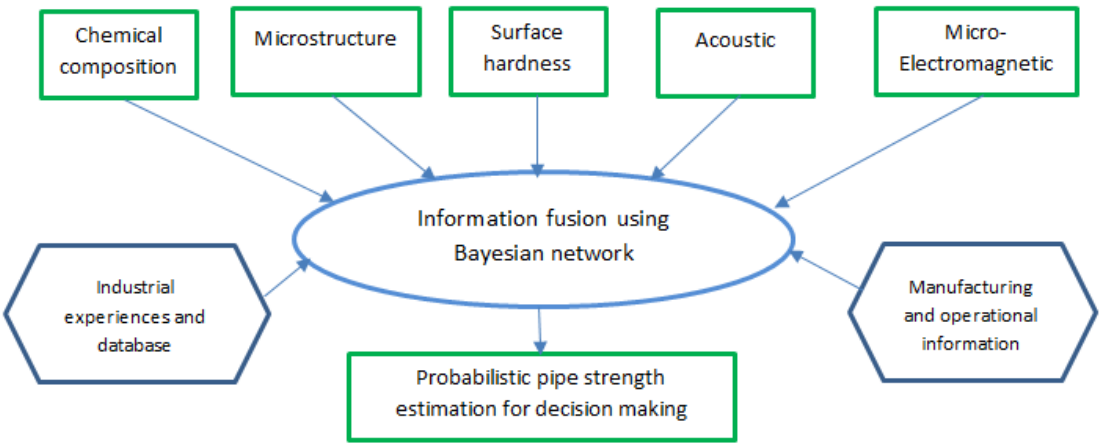

Figure 1.a): Schematic illustration of the proposed pipe strength estimation framework

(b) Status Update of Past Quarter Activities

<u>SECTION 1:</u>

<u>Task 1. Experimental testing and data analysis of chemical, metallurgical, and mechanical properties of pipe steel</u>

Summary

Several literature studies were carried out as a part of the previous quarters activities to understand the generic behaviour of the present system under study. This included studying the chemical and mechanical properties, such as composition, microstructure, stress-strain behaviour etc., for the different grades of linepipe steel and obtaining the statistical correlations were obtained between Yield strength and material properties. In the present quarter, this has been further extended to obtain the statistical correlations between Tensile Strength and the different material properties viz chemical and microstructural, to be used as likelihood functions in the Bayesian network fusion model.

And finally, methods for in-situ investigation of the toughness were in development, through the design of an ABI fixture.

Also, following on from the previous quarter activities, the different experiments conducted on the service linepipe steel samples obtained from GTI from one particular year of manufacturing, have been extended to another sample from a different year. The experimental testing consisted of metallographic inspection through Optical/SEM, image analysis through Image J software, composition analysis through EDS and Hardness tests with the Leeb Ball Hardness Tester. To add to these, tensile test of flat strip specimens was also conducted. The experiments were conducted for different thickness of the samples in order to capture the material property variation from the surface to the bulk, and an Ultrasonic thickness gauge was used to verify the thickness for the same. Another direction explored as a part of this study was to look into microstructure-property based model, in order to capture the mechanical property variation from surface to bulk with the help of a 3-D stochastic reconstruction model. And finally, the preliminary Bayesian Network model was further improvised to integrate the different components and provide a more accurate estimate of the probabilistic pipe strength and toughness.

Content

Samples from GTI:

The following service pipeline samples were obtained from GTI, as mentioned earlier, with the information of the installation year. The suspected grade and corresponding microstructures were obtained from the literature, based on the year of installation [1]. Two of these samples (pipe no. 45 & 47), marked with a highlighting have been used for the present study.

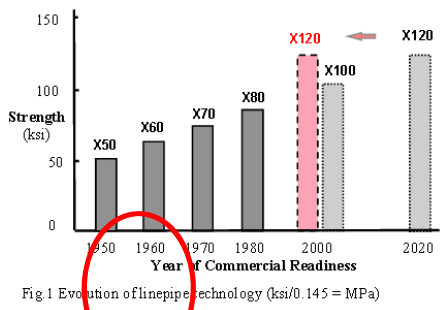

Figure:1 Development of pipeline steels [1]

Table1: Pipe samples and suspected grades

Pipe Number	Installation year	Pipe grade	Suspected grade	Suspected microstructures

24	2004	1522H	X100	BAINITE + MARTENSITE or bainite laths and M/A packets
32	1958	1522H	X60-X70	FERRITE PEARLITE
35	1961	1010	X60	FERRITE PEARLITE
44	Unknown	1513		Unknown
45	1949	1525	X50	FERRITE PEARLITE
47	1964	1025	X60	FERRITE PEARLITE

Experimental testing

1. **Microstructure Examination:**

1.a. Sample Preparation:

a. The sample under investigation was obtained from **Pipe Number 45 and 47**.
b. Flat samples were carved out of the curved pipe; Cross-section -10mm x 10mm, thickness -1mm, 2mm…outer diameter.
c. Samples were polished using Metallographic guidelines on the Silicon carbide papers and diamond cloth for finishing.
d. Thickness gauge was used to verify the sample thickness.
e. Samples were etched in 2% Nital solution for about 10-20 seconds.
f. SEM was used to obtain the microstructures.

1. b.Thickness Gauge Setup:

Figure 2: Thickness gauge set up

2. SEM analysis results:

2.a. Microstructure Images:

The samples were scanned in the thickness direction for microstructure examination. Pipe 45 (Figure 3) and Pipe 47 (Figure 4) yield the following microstructures on moving from outer diameter to inner surface.

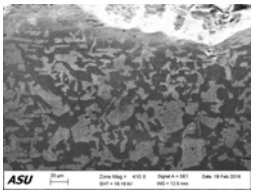

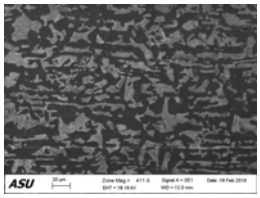

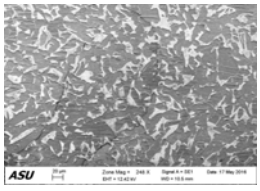

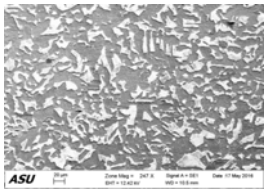

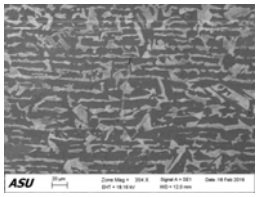

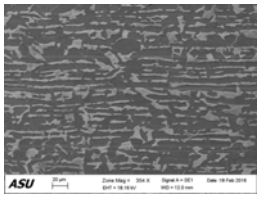

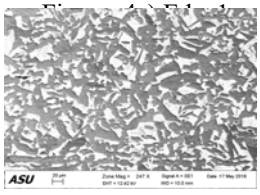

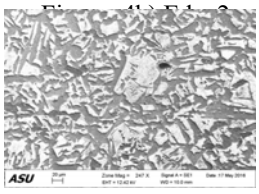

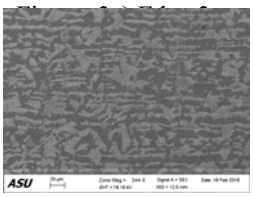

Figure 3e) Edge 5

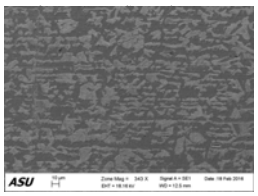

Figure: 3f) Edge 6

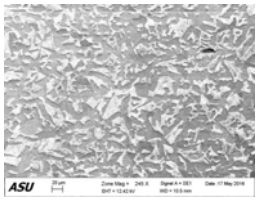

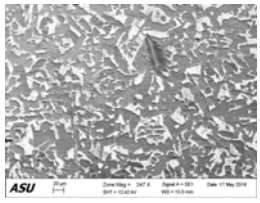

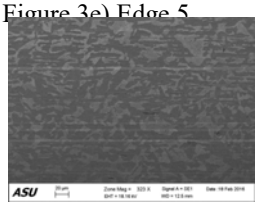

Figure: 3g) Edge 7

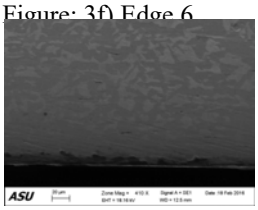

Figure: 3h) Edge 8

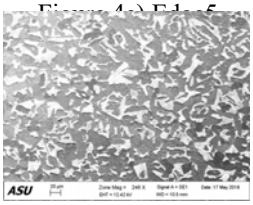

Figure: 4g) Edge 7

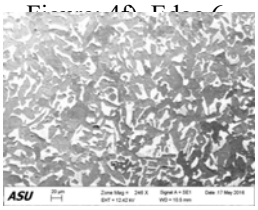

Figure: 4h) Edge 8

As the sample is traverses along the thickness for pipe 45, it can be seen that the micrographs in the middle region (figure 3d- 3f) depict a certain texture i.e. the phases are elongated along one direction (transverse). Cooling rate may have caused such a trend. But in general, usually the surface micrographs develop a texture due to fast cooling, in contrast to the present scenario. It is therefore, hard to say at the present moment, as to what may be the exact cause to generate such a trend for the system under study.

The samples from the second pipeline segment (pipe 47) did not a significant change in the microstructure while traversing through the thickness, which may be incorporated to different service duration of the installed pipeline system.

2.b. Volume fraction:

Next, Image analysing software Image J was used for quantification of area fraction of the two phases in the ferrite/pearlite system. The analysis is done corresponding to each image for the two specimens, to investigate for any possible trend along the thickness. The following charts are representative of the same.

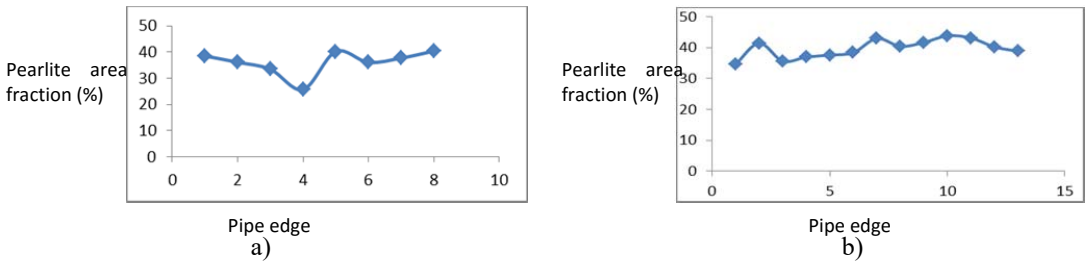

Figure.5. Plots showing thickness variation of phase percentages. a) Pipe 45 & b) Pipe 47

The plots show a slight trend in the pearlite area fraction for one of the samples whereas an irregular variation is observed for the other. The cause of the slight trend for Pipe number 45, also apparent visually from the images, is still under investigation.

Pipe 47 however, had a very ambiguous behaviour in terms of a possible trend, which again may be a result of a difference in the pipeline grade due to different year of installation and material properties.

3. Hardness:

The **Leeb Ball Hardness Tester** was used to examine the hardness of the samples, in order to determine the surface variation of hardness.

Table 2: Hardness of the pipe samples (HV)

Samples Thickness (mm)	Hardness (HV) H1	Hardness (HV) H2	Hardness (HV) H3	Mean Hardness (HV)
2	138	182	161	160.33
4	237	223	234	231.33
6	203	191	181	191.67

As can be seen clearly, the hardness of the samples in the middle region, with sharper phase morphologies, is higher, compared to the surface region of either edge. This can also be considered in line with the region exhibiting a certain texture, which presumably imparts a high value of hardness, or even corresponding higher value for strengths.

Figure 6a) Hardness tester

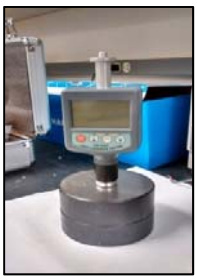

Figure 6b) Testing setup

4. EDS Analysis:

In order to obtain the chemical composition of the pipeline segment, semi-quantitative EDS was conducted on the samples with EPMA - JXA-8530F (JEOL), which resulted in a percentage composition for certain elements of interest.

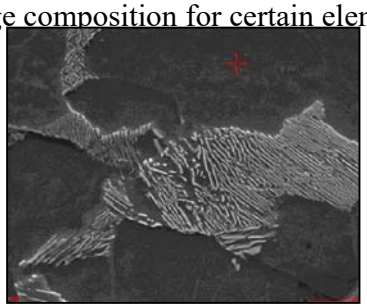

Figure 7a) SEM Image

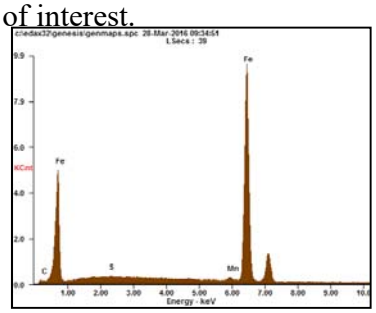

Figure 7b) EDS Spectrum

The beams were pointed at both the white and dark regions corresponding to Ferrite and Pearlite and the results were merged to obtain a quantitative weight percentage average. Below are the results from spot analysis of pipe 45, in order to match the possible trend in microstructure to that of the chemical composition.

Table 3: Composition (Weight percentage)

Distance from the outer diameter edge (mm)	Elemental Composition (%)								
	Fe	C	N	Si	V	Cr	Mn	Ni	Mo
0.6	96.84	1.37	0.24	0.11	0.03	0.03	1.23	0.30	0.14
1	97.52	0.99	-	0.13	0.03	0.06	1.28	0.26	0.11
1.5	97.23	1.05	-	0.07	0.02	0.03	1.26	0.29	0.10
2	96.29	1.74	0.5	0.1	0.03	0.08	1.28	0.27	0.09
3	96.51	2.72	0.21	0.08	0.01	0.03	1.24	0.21	0.06
3.5	97.47	1.43	-	0.07	0.03	0.03	1.19	0.24	0.10
4	94.84	3.43	0.06	0.06	0.03	0.01	1.20	0.30	0.12
5	96.83	1.46	0.09	0.05	0.03	0.03	1.32	0.25	-
5.5	97.17	1.11	0.07	0.05	0.05	0.03	1.31	0.24	0.03

The elements of interest were chosen based on their direct or indirect correlation to the strength and and toughness, obtained from literature, governed by certain equations. The primary elements of interest were Fe, C, N, Si, V, Cr, Mn, Ni and Mo, however some of these were observed to be present only in trace amounts and were accounted for reference. As the sample was traversed through the thickness, for observance of elemental composition, a considerable variation is not observed for the same. The trace elements such as Si, V, Cr, Mo however maintained a detectable range with Nitrogen not being detectable at certain spots. The weight percentage of Carbon, the most primary element of interest, did seem to fluctuate a little bit, with spikes around the middle section. The cause of such a behaviour and the possible link with the microstructure trend is still under investigation. The next step in this experimental study would be to perform a similar analysis for the other pipeline samples, starting with pipe 47.

5. Tensile Test

In addition to the EDS analysis, tensile test was conducted of the samples from pipe number 45, to measure mechanical properties of the given steel specimen and investigate the material-property relationship.Tensile test procedure conformed to the requirements of API 5L [2]. Flat strip tensile test specimens were carved out of the pipe specimens for this purpose.

As per the standard, specimens were cut in hoop orientation (parallel to the direction of maximum stress), as shown in the figure. The design geometry of tensile test specimens is demonstrated in Fig. 2. Flat transverse test samples had gauge width, thickness, and length of 38.1, 14.3, and 50 mm, respectively. It should be noted that flat strip samples were extracted from the entire thickness range of the pipe specimen to accurately capture material properties variation in the z-direction. With the given total thickness of the sample being 7.8 mm, four flat strip tensile specimens of 1 mm thickness were extracted out from inner diameter portion to the outer diameter edge.

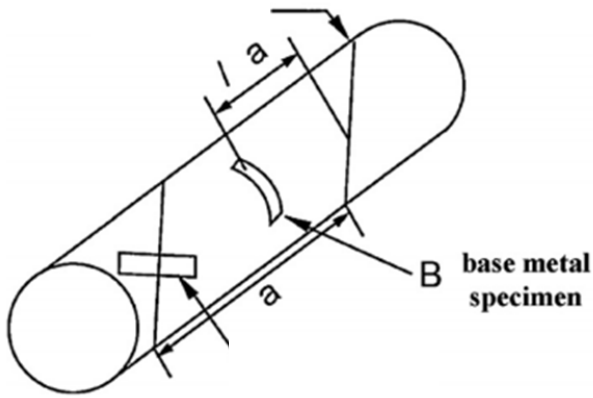

Figure.8. Orientation of flat strip tensile specimen within the pipe sample [9].

The test equipment employed for this purpose was a small scale tensile stage machine, to be able to successfully support the flat strip samples and measure the mechanical properties. All tensile experiments were conducted at room temperature under displacement control with a strain rate of 0.05 mm/s. In each test, the applied load and specimen elongation were measured. Results were obtained in terms of yield strength (at 0.5% total elongation according to API 5L), ultimate tensile strength (UTS), and specimen elongation (in 50 mm gauge length) at fracture point for each test.

The following table and chart lists the results obtained from the four samples.

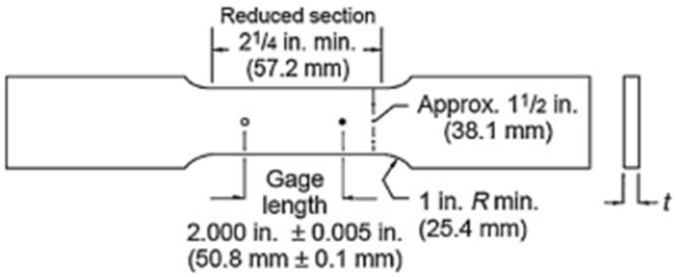

Figure 9b. Dimensions of flat strip tensile specimens

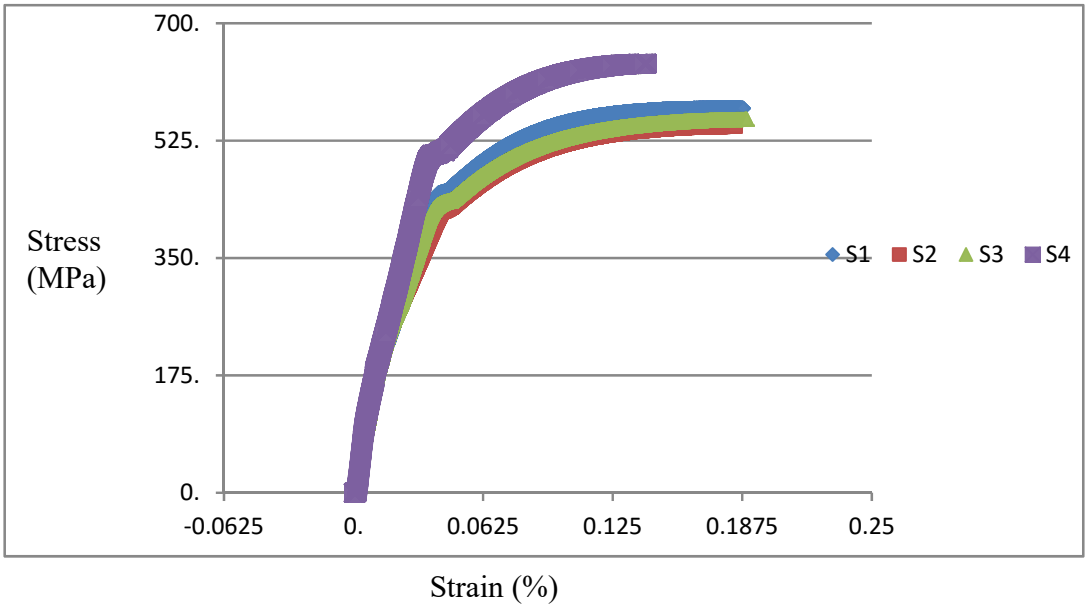

Figure.9a. Stress-Strain plot for the tensile test data

Table 3: YS and UTS of the samples

Samples	YS	UTS
S1	450	572.99
S2	425	538.4
S3	435	555.6
S4	506	637.5

The samples were labelled from S1 to S4 starting from the top to the bottom edge through the thickness. It can be seen that the samples from the inner and outer surfaces depict a Yield and Tensile strength higher as compared to the middle sections, which can be correlated to the microstructure patterns in the different regions. This will be further investigated and studies on hardness will be performed to further confirm the assertion behind the observed trend.

6. 3D Stochastic Reconstruction:

The procedure for the final part of 3-D reconstruction is demonstrated with an example, to be replicated in the present system. The methodology used for this is based on the stochastic reconstruction scheme developed by Yeong and Torquato [3]. Key structural features, known as statistical descriptors are extracted from the 2D images that

can contain various correlation functions. A typical 2-point correlation function for a statistically inhomogeneous system is;

$$S_2^{(i)}(\mathbf{x}_1,\mathbf{x}_2) = \left\langle I^{(i)}(\mathbf{x}_1) I^{(i)}(\mathbf{x}_2) \right\rangle = S_2^{(i)}(|\,\mathbf{x}_1 - \mathbf{x}_2\,|) \tag{8}$$

Where x_1 and x_2 are two arbitrary points and $S_2^{(i)}(x_1,x_2)$ is the probability of finding the two points in the same phase. A state of minimum "energy" is then computed from the given set of local minima, by the phase pixel interchange procedure in the digitized media. This energy is the sum of the squared difference of the reference and simulated correlation functions.

$$E = \sum_i \left[f_s(r_i) - f_0(r_i)\right]^2. \tag{9}$$

Where, $f_0(r)$ is the known two-point correlation function of the reference system, and $f_s(r)$ of the reconstructed digitized system, with r being the distance between two points in the system. The resultant energy from the phase interchange method is obtained as E', with the energy difference as E-E'. The probability of the phase interchange given by the Metropolis method is given as

$$P(E_{old} \rightarrow E_{new}) = \begin{cases} 1, & \Delta E < 0 \\ \exp(-\Delta E / T), & \Delta E \geq 0 \end{cases} \tag{10}$$

Where T represents temperature, and is adjusted with the simulation annealing method to converge the energy to a global minimum.

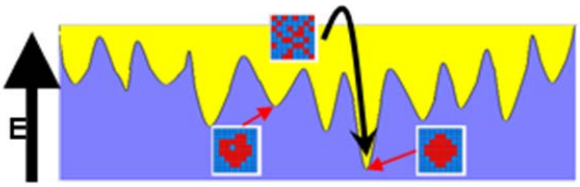

Figure.10.a The local minima, with the arrow towards the global minimum

A demonstration example to obtain the 3-D reconstructed model using the above procedure is as follows;

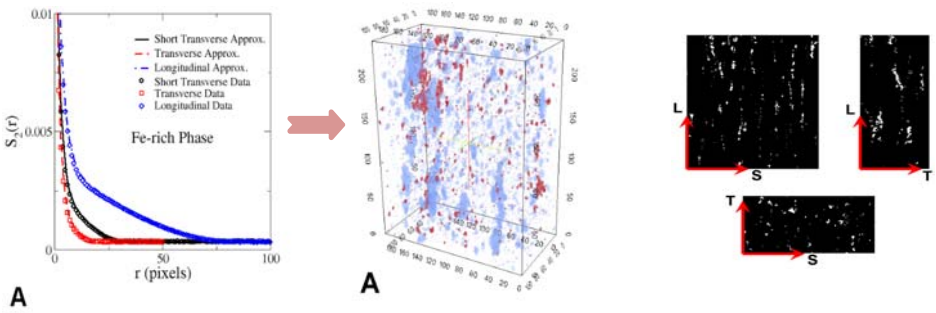

a) b) c)

Figure.10.b a) 2D correlation function, b) 3D reconstruction, c) Axes system

Task 3. Bayesian network for information fusion and probabilistic pipe strength estimation

The Bayesian Network model, developed with the use of an open source software WINBUGS, was further modified for probabilistic yield strength and Ultimate tensile strength prediction. This is based on the general Bayes theorem [4]:

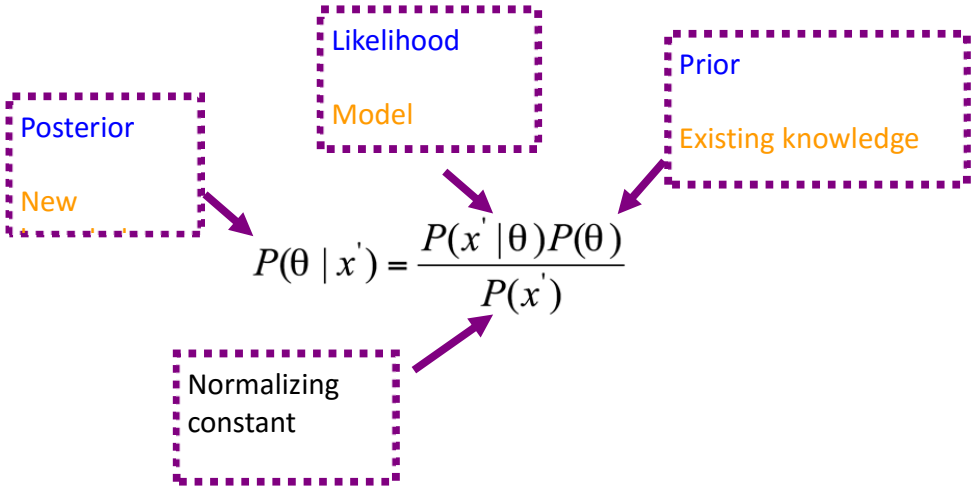

The following correlations between YS, UTS and the different material properties have been utilized;

YS= 53.9 + 32.34(Mn) +83.2(Si) +354.2(N_f) + 17.4 (d -1/2) [5]

where Mn – Mn content (%), Si – Si content (%), N_f - free N content (%), and d - ferrite grain size (in mm)

YS(f/p)= YS(f) (V_f) + YS(p) (1-V_f) [6,7],

Where YS(f/p) is the yield strength of the dual phase material, YS(f) is the yield strength of the ferritic phase and YS(p) is the yield strength of the pearlite phase. Vf is the volume fraction of ferrite.

YS=2* H+105 [8], where H - Vickers hardness

Also, TS = 1.3 × H + 344 [8], where H-Hardness

TS = 294.1 + 27.7(Mn) + 83.2(Si) + 3.9(P) + 7.7(d-2) [5], where P is the pearlite content in the matrix and the other symbols have the usual meanings.

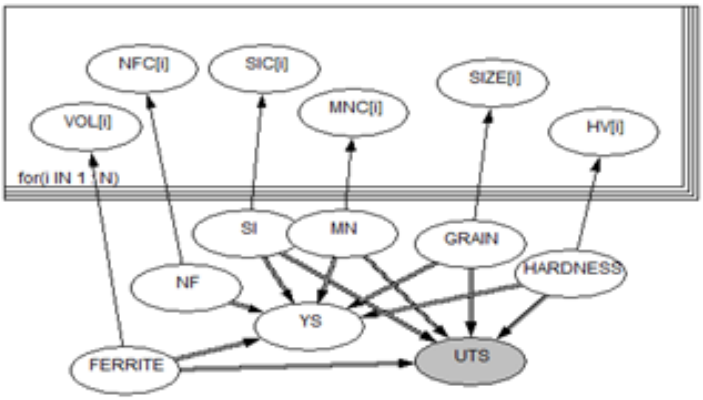

Figure.11. BN Model for YS and UTS determination

This model was developed step by step by increasing the strength dependence of the Nodes. As a part of the preliminary study, equal weights were assigned to all the nodes, which can be modified based on the results. Data was fed at each step and YS and TS was estimated to validate the integrity of the model, as shown in table.

The data used for this purpose is a combination of literature sources (Nf content, Ferrite grain size), and the experimental data (Hardness, Mn, Si, C content etc.)

A series of data was provided which can be handled with the loops in the present system. The model uses one data at a time and estimates a posterior distribution for the give YS/TS measurements, which forms the prior for the subsequent iterations, as shown in Table 4.

The lower bound Yield strength for API X52 pipes is typically around 360 MPa.

Table 4: Bayesian nodes updating

Updating Node	YS Mean (MPa)	Std. Deviation
Hardness [8]	496.0	45.24
Hardness-grain size-composition [8]+[5]	388.8	45.51
Hardness-grain size-composition-phase volume [5] + [6] + [7] + [8]	447.5	36.44

This suggested that different weights have to be assigned to the different nodes, for better convergence.

Following this, trial and error method was used to assign different weights to the nodes, to improve the mean value close to the realistic one and to reduce the standard deviation. For example, updating the weightage of the node Ferrite volume percentage to 1/5 leads to a YS mean value of 368.4 MPa, Stdv= 33.98, which shows that appropriate weightage can have a significant impact on the system convergence.

Another important feature of the present BN model is that all the nodes can be updated based on the measurement provided for one or more nodes in the system, with/without direct dependence on the measurement nodes. For example, the mean and SD for the node SI, changes from 0.46, SD= 0.19 to 0.435, SD= 0.201 in the absence of measurement for the node Hardness. This helps in converging the parameter values and quantifying the uncertainty of the system as the model is updated in the view of new information from various measurements [9].

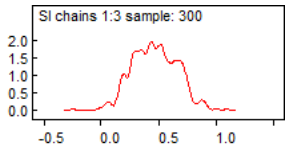

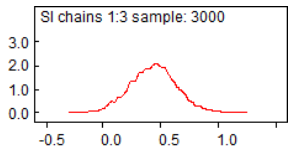

Figure.12a) With measurement 12b) Without measurement

References:

1. J.Y.Koo,M.J.Luton,M.V.Bangan,R.A.Petkovi. Metallurgical Design of ultra-Strength steel for Gas pipeline.

2. API Specifications 5L, Specifications for line pipe, forty-third ed., American Petroleum Institute, 2004.

3. C. L. Y. Yeong and S. Torquato, Phys. Rev. E 57, 495 (1998).

4. Liu, W., K. Yue, and J. Zhang, Augmenting learning function to Bayesian network inferences with maximum likelihood parameters. Expert Systems with Applications, 2009. **36**(2, Part 2): p. 3497-3504

5. Bruce L. Bramfitt (1998). Structure/Property Relationships in Irons and Steel, *Bethlehem Steel Corporation. ASM International.*

6. Thomas Hoper.Shigeru Endo.Nobuyuki Ihikawa and Koichi Osawa (1999). Effect of Volume Fraction of Constituent phases on the stress-strain relationship of Dual Phase Steels. *ISIJ International, Vol. 39.*

7. Zhonghua Li a, S. Schmauder b, M. Dong b. A simple mechanical model to predict fracture and yield strengths of particulate two-phase materials. *Computational Materials Science 15 (1999) 11-21*

8. S.H. Hashemi (2010). Strength–hardness statistical correlation in API X65 steel, *Materials Science and Engineering A 528 (2011) 1648–1655*

9. Ma, Y., Wang, L., Zhang, J., Xiang, Y., Peng, T., and Liu, Y. (2014). "Hybrid Uncertainty Quantification for Probabilistic Corrosion Damage Prediction for Aging RC Bridges." *J. Mater. Civ. Eng., 10.1061/(ASCE)MT.1943-5533.0001096, 04014152.*

SECTION 2:

Design of Automated Ball Indentation test equipment:

1. Introduction:

The United States transports liquid petroleum over 190,000 miles whereas the natural gas pipeline system is a massive underground network of over 2.4 million miles [1]. About 67% of the total crude oil pipelines were laid down before 1980 [2]. Over a period of time, due to the internal as well as external conditions of the pipelines, they deteriorate gradually. The integrity of the pipeline is important to avoid leakage, leading to safety and environmental hazards and tremendous losses. Conventional mechanical tests require large test specimens, which may not be feasible for pipes in service. Therefore, it is of great importance to develop methods which can be performed in-situ. Since the testing is carried out in-situ, it needs to be non-destructive or minimally destructive in order to serve the purpose of testing [4]. The automated ball indentation (ABI) test is based on strain-controlled multiple indentations (at the same penetration location) of a polished surface by a spherical indenter (0.25 to 1.57-mm diameter). The microprobe system and test methods are based on well demonstrated and accepted physical and mathematical relationships which govern metal behaviour under multiaxial indentation loading [5]. The objective of the research project is to predict the through thickness mechanical properties (toughness, yield strength, ultimate tensile strength etc.) of a material specimen using ABI testing.

2. Previous Work:

An electromechanical MTS testing machine, capable of a maximum loading of 10kN is used to carry out the ABI testing. Fixtures to hold the indenter and specimen were designed for the machine. The displacement and load of the indenter can be monitored via Testworks software by MTS. A MATLAB code to obtain the stress-strain curve from experimental data has been written. In order to validate the code, the stress-strain curve is compared with literature data for stainless steel by Fahmy Haggag et. al [4]. A finite element model to simulate the testing has been generated with a single loading case for the indentation in the plate specimen.

3. Post-processing Experimental Data:

The testing data yields the load displacement curve for a given specimen. However, this data needs to be converted into the stress strain curve in order to estimate the yield strength and ultimate tensile strength of the material. The equations relating the indentation depth and load to the true stress and strain are developed from the geometry of the indenter and the indentation on the test specimen [5]. The system of non-linear equations which need to be solved in order to obtain the true stress and strain from the load and displacement can be given as shown in Figure 1.

$$\varepsilon_p = 0.2\, d_p / D$$

$$\sigma_t = 4P / \pi d_p^2 \delta$$

where

$$d_p = \{0.5\, CD[h_p^2 + (d_p/2)^2] / [h_p^2 + (d_p/2)^2 - h_p D]\}^{1/3}$$

$$C = 5.47P(1/E_1 + 1/E_2)$$

$$\delta = \begin{cases} 1.12 & \Phi \le 1 \\ 1.12 + \tau \ln \Phi & 1 < \Phi \le 27 \\ \delta_{\max} & \Phi > 27 \end{cases}$$

$$\Phi = \varepsilon_p E_2 / 0.43\sigma_t$$

$$\delta_{\max} = 2.87\alpha_m$$

$$\tau = (\delta_{\max} - 1.12) / ln(27)$$

Figure 1 system of non-linear equations which need to be solved [5]

The notations given in the figure above represent the quantities as given below:

ε_p = true plastic strain induced in the test specimen

d_p = plastic deformation diameter

h_p = plastic deformation height

D = indenter diameter

P = load

δ = parameter whose value depends on the stage of development of the plastic zone beneath the indenter

Φ = indentation variable

E1 = Young's modulus of the indenter material

E2 = Young's modulus of test specimen material

α = constraint factor index

σ_t = true stress

The code was tested using load-displacement values from literature [4]. The assumptions made while formulating the problem in MATLAB are as follows:

1. Young's modulus for both indenter (E = 550*10^3 MPa) and test specimen (250*10^3 MPa)
2. Constraint factor index (0.03-2.6)

The stress strain plots obtained from the method followed above are shown in Figure 2.

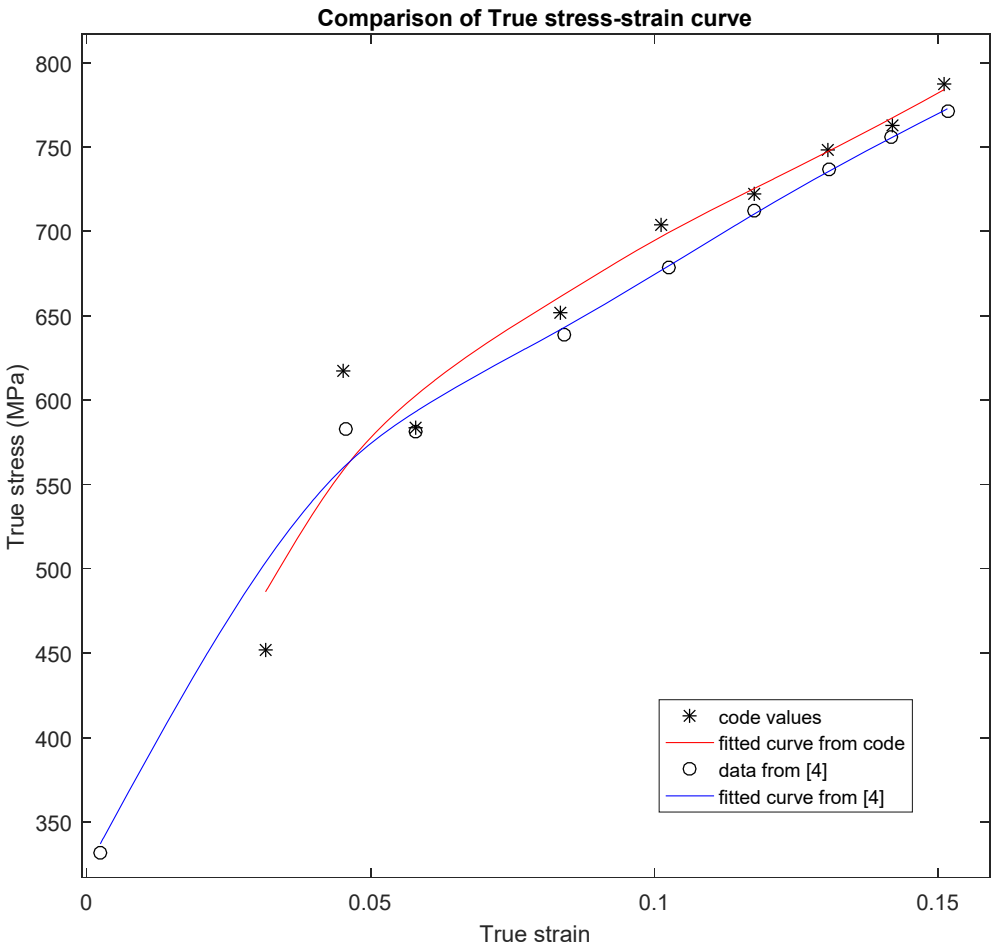

Figure 2 Comparison of stress-strain plot from literature with the coded MATLAB plot

There are various possibilities for the difference in the values obtained from the code and literature. The material properties such as the Elastic modulus for the indenter and material may not be the same for the stress strain curve from literature. However, both the curves obtained from the methods are similar in nature and comparable. A slight error might occur while digitizing the literature data to obtain the load-displacement as well as the actual stress-strain points. In order to validate the post-processed testing, a simulation is carried out in ABAQUS.

4. Finite Element Model:

The geometry of the indenter and plate is modelled in ABAQUS as shown in Figure 3, along with the loading conditions. The indenter is considered to be an analytical rigid body, given its high hardness and the plate material is considered to be steel with elastic-plastic deformation occurring due to the contact. The material properties used for the steel plate are summarized as given below:
Modulus of Elasticity – 210.7GPa
Poisson's Ratio – 0.303

Yield stress (MPa)	Plastic Strain
200.2	0

246	0.02353
294	0.0474
374	0.09354
437	0.1377
480	0.18

Table 1. Plastic properties for steel

Boundary conditions are applied on the plate and indenter so as to simulate the contact of the pair. The bottom face of the plate was fixed and the load is applied on the top face of the indenter. The boundary conditions applied are shown in Figure 4. While defining the contact pair, the plate is made the master surface whereas the indenter is considered as the slave surface.

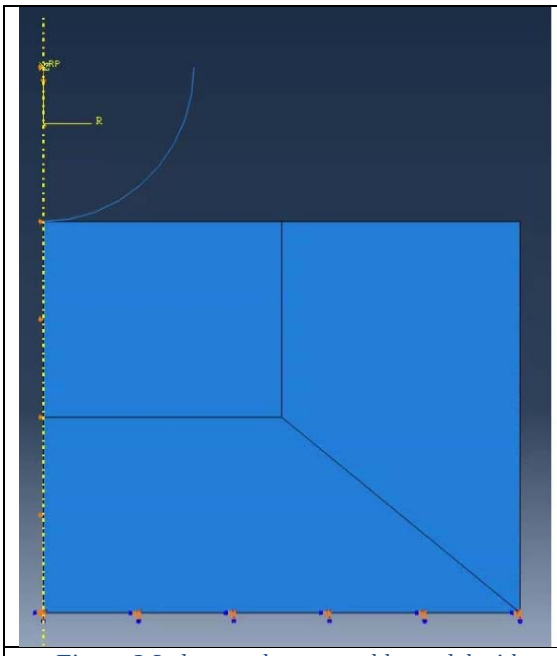

Figure 3 Indenter-plate assembly model with loading and boundary conditions

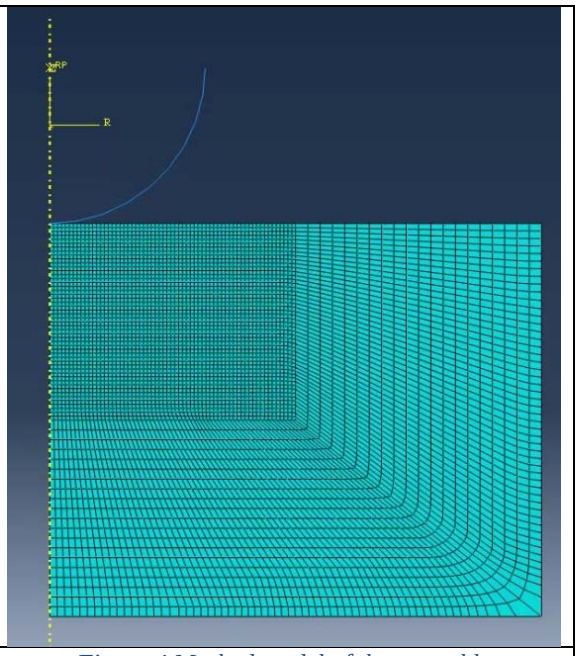

Figure 4 Meshed model of the assembly

The model was meshed using various control parameters such as edge divisions to achieve good quality elements in the desired region. A displacement controlled loading-unloading curve with 6 cycles is simulated. The loading and unloading steps data is as shown in Figure 5. From, the simulation, it can be seen that the plate relaxes slightly in the unloading cycles, retaining the plastic strain in the plate specimen.

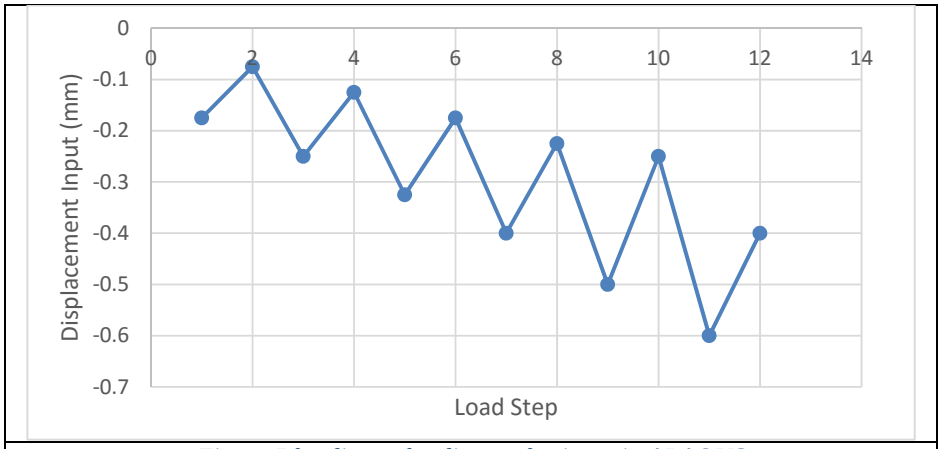

Figure 5 loading unloading cycles input in ABAQUS

The maximum residual deformation in the plate after the final unloading step is as shown in Figure 6 whereas the residual stress in the plate after unloading is as shown in Figure 7. A video of the simulation can be seen in the link: https://youtu.be/5qHptM73Fmo

A simulation for actual ABI testing data needs to be carried out to validate the testing stress-strain curve obtained from the MATLAB code.

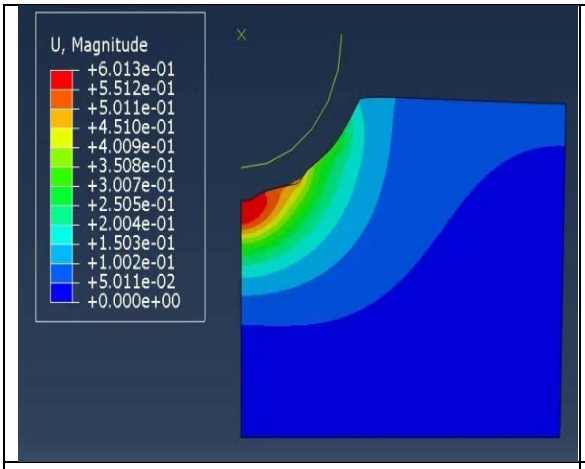

Figure 6 displacement plot after the final cycle

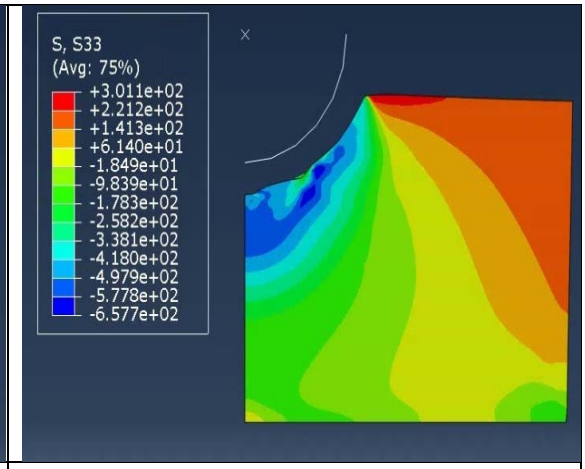

Figure 7 Stress plot after the final cycle

5. Future Scope:

- Validation of the FEA model using the stress-strain curve obtained from MATLAB code generated. A variation in the material properties for the pipe specimens at various depths to obtain the stress-strain curve.
- Validating the testing model with simulation for the variation in through thickness material properties.

References:

[1] American Petroleum Institute: http://www.americanpetroleuminstitute.com/Oil-and-Natural-Gas-Overview/Transporting-Oil-and-Natural-Gas/Pipeline

[2] Inside Energy: http://insideenergy.org/2014/08/01/half-century-old-pipelines-carry-oil-and-gas-load/

[3] Das, M., Pal, T. K., and Das, G., 2012, "Use of Portable Automated Ball Indentation System to Evaluate Mechanical Properties of Steel Pipes," Trans. Indian Inst. Met., **65**(2),

pp. 197–203.
[4] Haggag, F. M., 1993, "In-situ measurements of mechanical properties using novel automated ball indentation system," ASTM Spec. Tech. Publ., pp. 27–44.**SECTION 3:** Task 2. Experimental testing, data analysis and prototyping for acoustic and micro-electromagnetic properties of pipe steel

SECTION 3:

Task 1 – Scanning images deconvolution

Near-field microwave microscopy is very useful to identify and characterize injurious materials. However, a near-field microwave microscopy imaging system is not able to acquire a clear image directly because scanning images are blurred in the axial direction by contributions of point spread function. The results of scanning include not only the propriety of the materials but also the pattern of the antenna. In this quarter, we study image enhancement of scanning images by deconvolution.

Deconvolution is a computationally intensive image processing technique existing in a broad range of signal and image processing fields. It becomes necessary when we want to deburr image for a better performance or further processing. The high-frequency information usually contains the texture characteristic of the target. Due to the point spread function is the low-pass filter, the high frequency of image is suppressed and even lost. Since the image textures are important visual information for the human eyes to detect damaging location, the aim of deconvolution is to reconstruct the high-frequency part. However, the observation noise will be amplified, which means that the deconvolution results may vary from the real solution. Therefore, the deconvolution method should compromise between the performance of the scanning reconstruction and noise amplification.

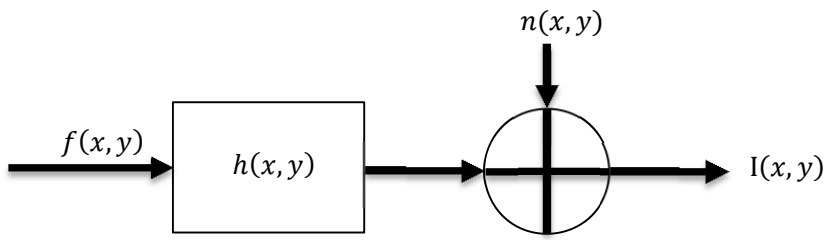

*Fig.*1 model of degraded image

The degraded images can be expressed as follow:

$$\mathrm{i}(\cdot) = h(\cdot) * f(\cdot) + n(\cdot)$$

I(t) is the image we acquire from the scanning, $h(x, y)$ is a pulse response of the linear system which is also known as point spreads function, and $n(t)$ represents noise. $f(x, y)$ is the physical quantity without distortion that we want to solve. If one of the functions $h(x, y)$ or $f(x, y)$ is known, we can use Weiner filtering or iterative restoration to recover the other function. The problem is termed as blind deconvolution if neither $h(x, y)$ or $f(x, y)$ is known and only the output image i(x, y) is available.

<u>Task 1(a) – Point spread function estimation</u>

In order to solve the deconvolution and get the f(x, y), we first find an estimate of the Point spread function. The first estimate is based on the pattern of the antenna. We first generating a matrix to approximate the point spread function by the following equation:

$$E_\theta \cong -j\eta \frac{I_0 l e^{-jkr}}{4\pi k r^3} sin\theta$$

The size of the matrix is measured the blurred part around square on the scanning image.

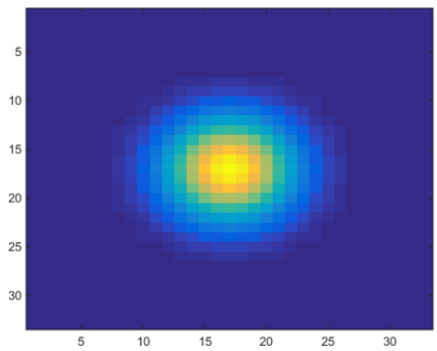

*Fig.*2 estimate of the point spread function

Since the estimation contains some very small value or even zero, and matrix is in the denominator during the calculation, we use the Weiner filtering to solve the deconvolution instead of divide directly.

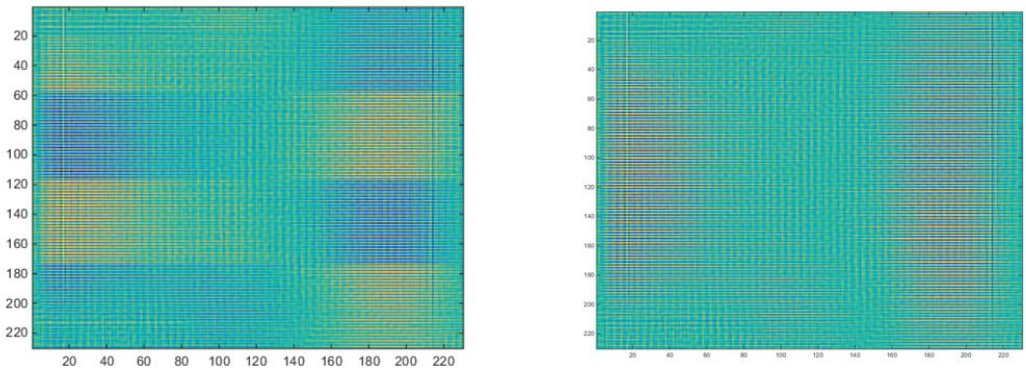

Fig.3 results of the deconvolution

To a certain extent, we can see the square in the figure 3. However, it is unclear and still very blurry. Another approach is estimating the point spread function by deconvoluting the f(x, y) from the i(x, y). Although f(x, y) is unknown and need to be solved, we can get an approximation $f'(x, y)$ by observing the scanning object. Then the point spread function estimation $h'(x, y)$ can be solved by the following equation if we ignore the noise.

$$h'(\cdot) = \text{ifft}(\text{fft}(\text{i}(\cdot))/\text{fft}(f'(\cdot)))$$

In the equation, fft and ifft represent fast fourier transform and inverse fast fourier transform respectively.

We scanned a PA board with a 1-inch by 1-inch square hole six times and stored the data as $i_k(x, y)$, k ∈ [1,6]. The scanning system acquires 200 data per inch which corresponding to 200 pixels in the image.

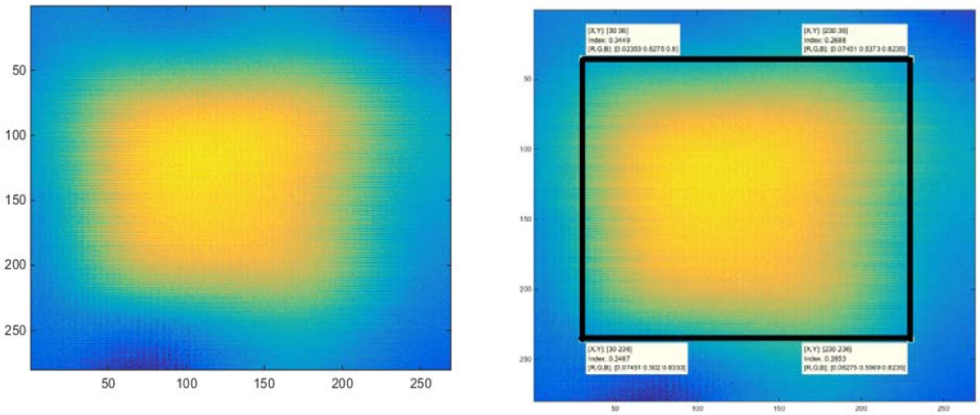

(a) (b)

Fig.4 (a) scanning image (b) approximate of the object vertexes

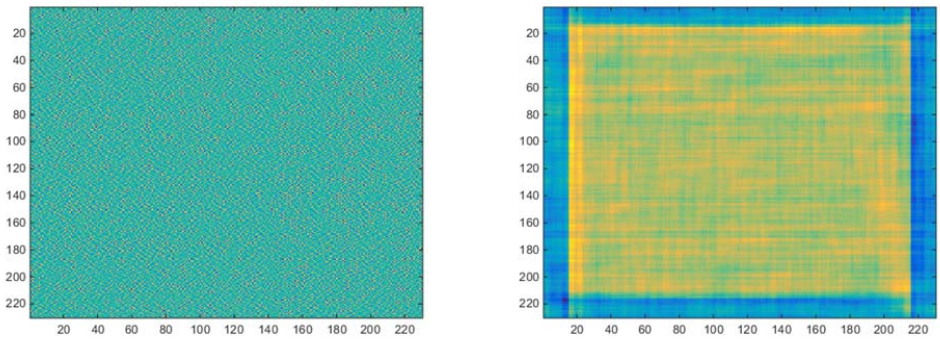

(a) (b)

Fig.5 (a) estimate of the PSF (b) reconstruct image by the $h'(x, y)$

We draw a 200 by 200 square on the corresponding location in the Matlab as the $f'(x, y)$. Then $h'_k(x, y)$ can be solved by equation. By averaging $h'_k(x, y)$ we can get the estimate of the point spread function. However, the result is not accurate since the poor knowledge about f(x, y). The f$'(x, y)$ we used may have a big difference from the actual physical quantity. The estimate of the point spread function need to be improved since the pattern should be central symmetry and have the greatest value at the center.

<u>Task 1(b) – Blind deconvolution</u>

Blind deconvolution is very complicated since we have to infer both the original object and the point-spread function. There are many methods and can be divided into two categories, statistical approach and deterministic approach. We study both two methods and in this quarter we

implemented one of the statistical deconvolution algorithm on the near-field microwave microscopy system.

Richardson–Lucy deconvolution algorithm is a statistical approach which based on the Maximum Likelihood and developed from Bayes's theorem.

$$\mathrm{P}(x|y) = \frac{\mathrm{P}(y|x)P(x)}{\int \mathrm{P}(y|x)P(x)dx}$$

The $\mathrm{P}(x|y)$ is the conditional probability of the event x when event y has happened. If we take the $P(x)$ as the physical quantity f(x) we want to solve, $\mathrm{P}(y|x)$ as the point spread function $h(y,x)$located at x and $P(y)$ as the scanning image $i(y)$, we can get the equation

$$f_{j+1}(x) = \int \frac{h(y,x)i(y)dy}{\int h(y,z)\, f_j(z)dz} f_j(x)$$

The j in the equation is the iteration number. If the point spread function is known, the f(x) can be solved by the following equation

$$f_{j+1}(x) = \left\{\left[\frac{i(x)}{f_j(x) \otimes h(x)}\right] \otimes h(-x)\right\} f_j(x)$$

Since we already know the scanning image i(x) and the point spread function $h(x)$, all we need to do is iterating the equation until convergence with an initial guess of the $f(x)$.

In the blind deconvolution both $h(x)$ and the $f(x)$ is unknown and need to be calculate in the previous iteration.

$$h_{j+1}{}^{k}(x) = \left\{\left[\frac{i(x)}{h_j{}^{k}(x) \otimes f^{k-1}(x)}\right] \otimes f^{k-1}(-x)\right\} h_j{}^{k}(x)$$

$$f_{j+1}{}^{k}(x) = \left\{\left[\frac{i(x)}{f_j{}^{k}(x) \otimes h^{k}(x)}\right] \otimes h^{k}(-x)\right\} f_j{}^{k}(x)$$

We have implement this algorithm with the testing data. The value range of the scanning data is around -0.003. Therefore, in order to get the data prepared for the following process, we should First normalize the scanning data.

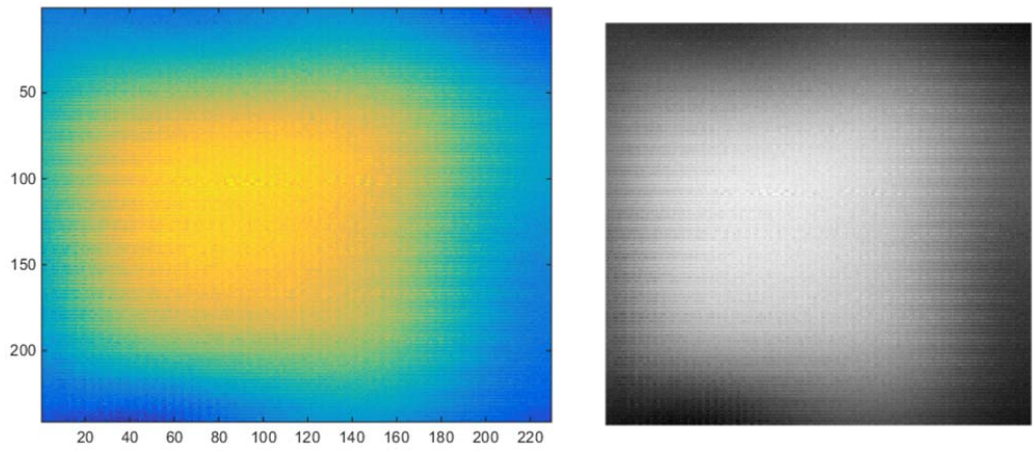

Fig.6 scanning result and normalized grayscale image

Then we should make an initial guess about the size of the point spreads function. The size of the point spreads function is critical and will have more effect on the result of the deconvolution. It can be determined by measuring the blurred part around a noticeably sharp object on the scanning image.

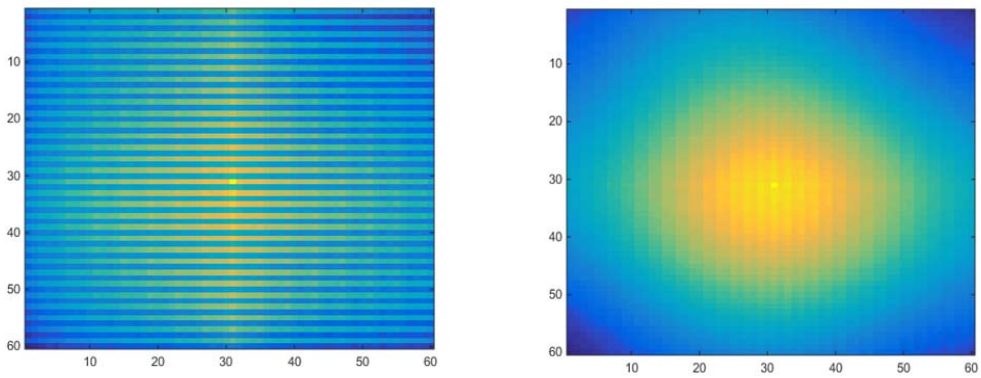

(a) (b)

Fig.7 (a) restored point-spread function (b) restored point-spread function from down-sampled data

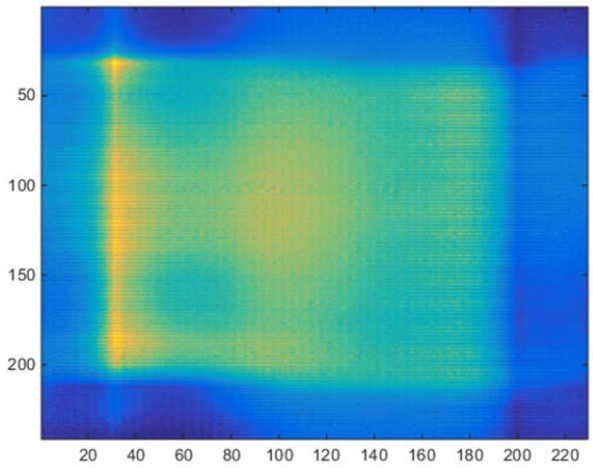

Fig.8 deblurred image

In order to improve the result of the deconvolution, a weight matrix has been generated by applying the edge detection. This will let the deconvolution process ignore the high contrast areas and the noise reduce relate to the contrast can be reduced.

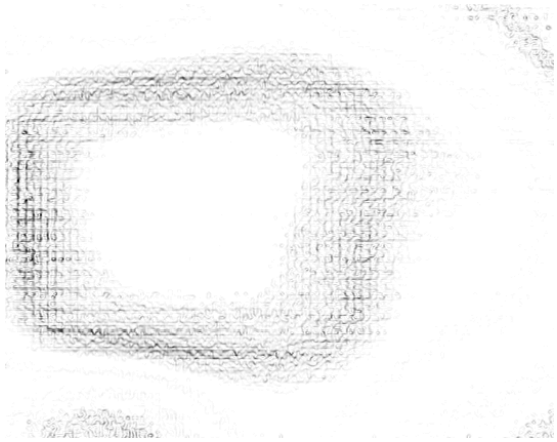

Fig.9 result of edge detect

The size of the weight matrix is same as the image. The high-contrast areas have been assigned the zero value and the corresponding pixels in the scanning result will be excluded from the deconvolution processing. The high-contrast areas can be detected by edge detection.

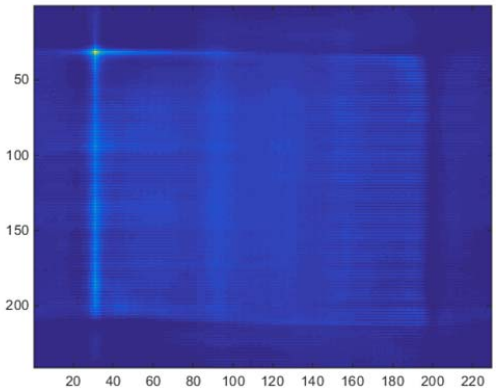

Fig.10 deblurred image with weighted

We can see the square in the figure shown above. In order to have a more obvious contrast, the image is converted to a black and white image

(a) (b) (c)

Fig.11 black and white image of (a) scanning result (b) deblurred image (c) deblurred image with weighted

From the figure 11 we can see that the result of the deconvolution suits the actual shape of object better than the original scanning result. It looks like a quadrilateral with straight edge and right angle. Further process is needed to improve the performance. More sample will be scanned and test the algorithm.

Task 2 -Correlations between DIC (mechanical properties) and NFMW (electro-magnetic properties)

We scanned some PE specimens and correlate the scanning results with DIC (mechanical properties) in the last quarter. In this quarter, we did more scanning include PA full specimens. The scanning results have been analyzed and compared with the DIC data.

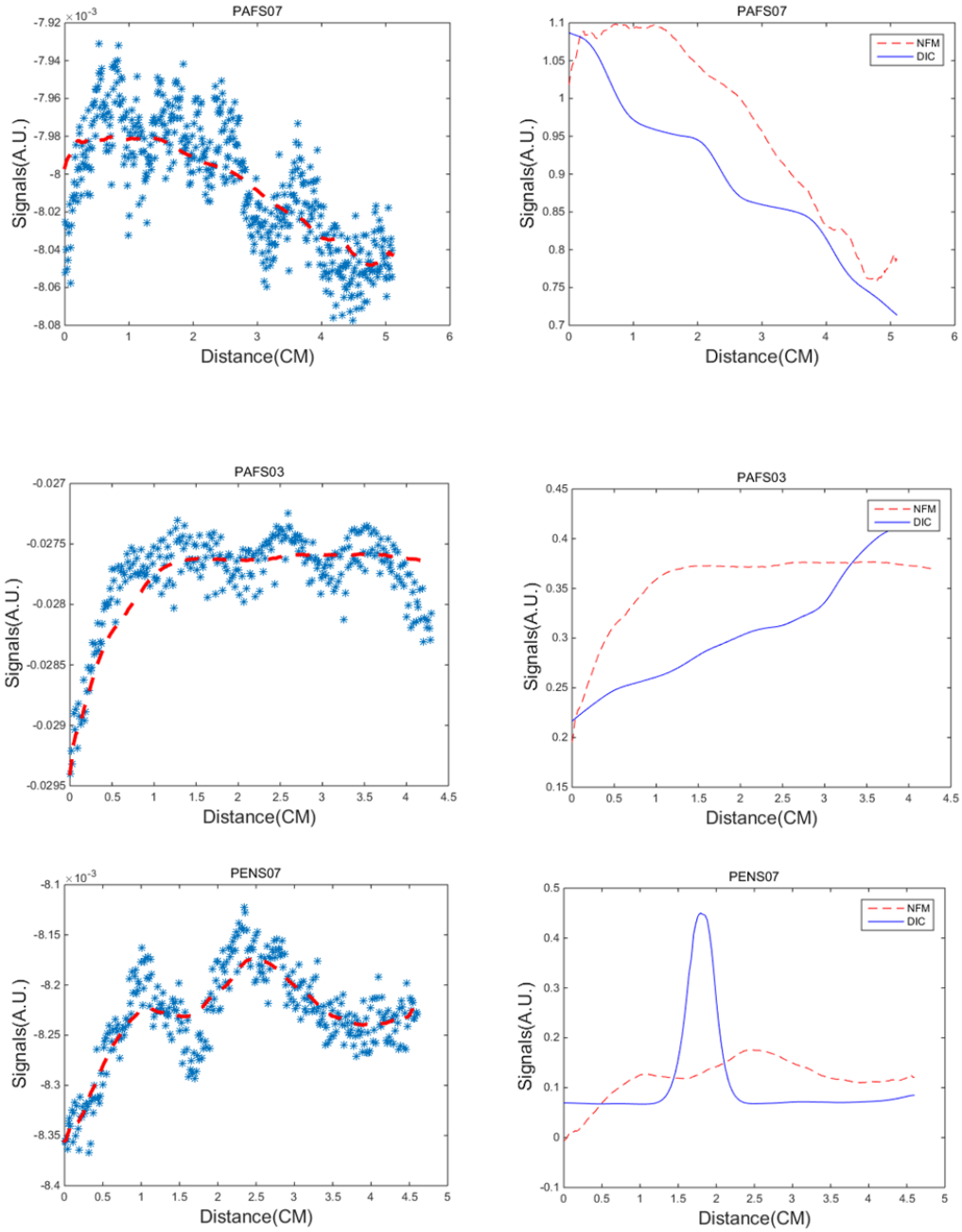
PAFS07
Signals(A.U.)
Distance(CM)
PAFS07
NFM
DIC
Signals(A.U.)
Distance(CM)
PAFS03
Signals(A.U.)
Distance(CM)
PAFS03
NFM
DIC
Signals(A.U.)
Distance(CM)
PENS07
Signals(A.U.)
Distance(CM)
PENS07
NFM
DIC
Signals(A.U.)
Distance(CM)

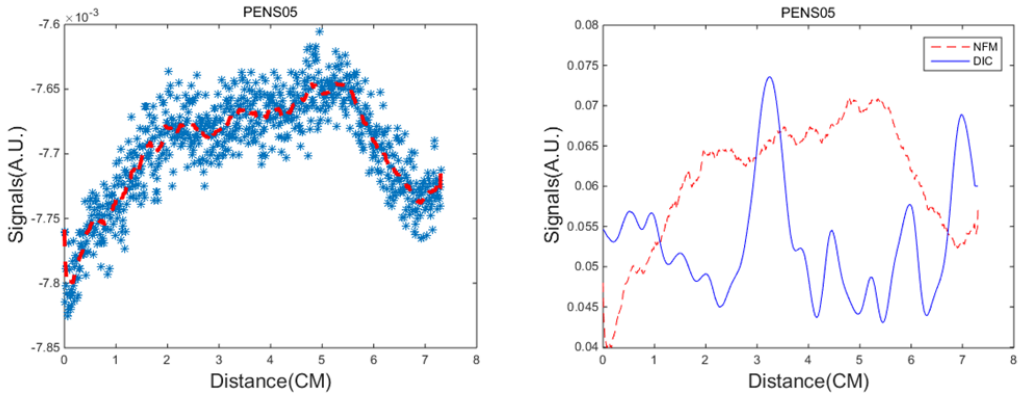

Fig.12 scanning results and correlation of the PA and PE specimens

The blue stars stand for the data from near field scanning, and the red dash line is the average of scanning data from nonstop near field scanning, and the red line is the DIC result from ASU tensile testing. For the notched specimens, we can see that trends of red lines and blue lines experience a quite different trend at the middle part where the hole located. For the full PA specimens, the trends of the red lines and blue lines are matching better when the specimens are elongate longer which shows same correlations results with full PE specimens.

In order to get a better understanding of elongating effect on the specimens, we get two digital optical microscopes which are able to capture images at 60x~200x and 500x~1000x respectively. We use the digital optical microscopes to observe the difference on the surface of elongated specimens and original specimen.

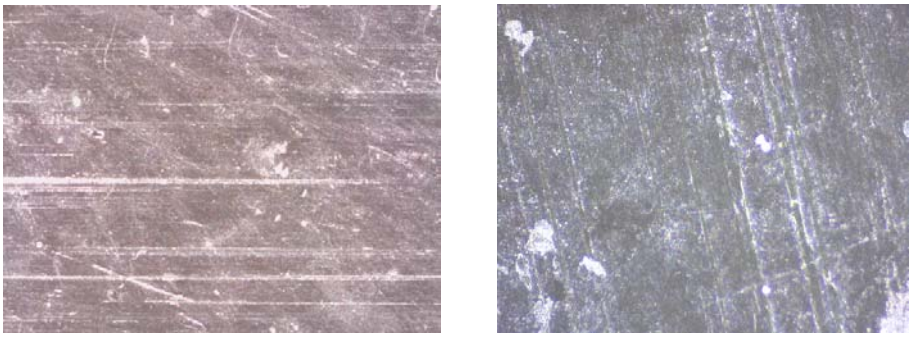

(a) (b) .

Fig. 13 image Magnified 682 times of (a) PA original specimen (b) PA 70% elongated specimen

From the pictures, we can see that elongated specimen has more vertical fissures on the surface. The distribution of the fissures on 70% elongated specimen is not uniform. We will try to correlation the distribution with other results in the next quarter.

Description of any Problems/Challenges

The project progress is satisfactory according to the schedule of the task table. Good communications between the PIs, students and program director is well maintained. No technical challenges were identified in this quarter.

Planned Activities for the Next Quarter

Besides the planned activities mentioned above, here are the future work for the next quarter Q4: ASU will continue the testing for material property characterization and Bayesian inference. Numerical simulation and experimental testing for ABI method will be further investigated. CU will continue to improve the sensitivity and resolution of the micro-electromagnetic imaging techniques assisted by multi-physics modeling. Pipe steel samples investigation will be carried out in Q4.